Welding in the World (2018) 62:885–892
https://doi.org/10.1007/s40194-018-0592-8

RESEARCH PAPER

Selective laser melting of AlSi10Mg alloy: influence of heat treatment condition on mechanical properties and microstructure

A. Iturrioz[1] · E. Gil[1] · M. M. Petite[1] · F. Garciandia[1] · A. M. Mancisidor[1] · M. San Sebastian[1]

Received: 13 July 2017 / Accepted: 26 March 2018 / Published online: 23 April 2018

Abstract
AlSi10Mg is the Al alloy most applied for selective laser melting (SLM) processing studies. The characteristics and the density obtained for SLM-processed material is extremely influenced by the quality of the starting powder. Since the microstructure obtained after SLM is often metastable, the required heat treatment to obtain an "optimized" microstructure can be significantly different than the one applied to conventionally cast or wrought Al alloys. In the present work, different thermal treatments have been applied to samples manufactured by SLM in order to investigate the effect on the microstructure and mechanical properties. The microstructural evaluation has been performed by SEM analysis and the mechanical properties have been determined by hardness measurements and tensile tests. Samples in the as-built condition, after stress relieving and under T6 heat treatment have been investigated to determine the best combination of properties.

Keywords Selective laser melting (SLM) · AlSi10Mg · Heat treatments · Microstructure · Mechanical properties

1 Introduction

The higher solidification rate achieved in the manufacturing of AlSi10Mg alloy by selective laser melting (SLM) (~ 10^6 °C/s) [1] in comparison with the traditional casting processes (less than 10^2 °C/s [2–4]) induces some changes in the microstructure such as its refinement and more homogeneous distribution of the Si-rich eutectic constituent. These changes have strong influence on mechanical properties, improving tensile strength and ductility [4].

AlSi10Mg is one of the most common Al alloys used in powder bed manufacturing technologies [5–7]. Its chemical composition provides appropriate properties to be manufactured and applied, mainly, in the aeronautics and automotive fields. Si content helps to improve laser absorption since Al has a very high reflectivity. This element also enhances the fluidity and reduces the solidification range, making this alloy more wettable [8] and easier to process by additive manufacturing. The addition of Mg allows the precipitation of Mg_2Si during heat treatments, causing the hardening of the matrix.

T6 heat treatments are usually performed with the purpose of enhancing mechanical properties of aluminum cast alloys [9]. Subjecting AlSi10Mg cast alloys to these treatments causes the precipitation of Mg_2Si phase, which lead to material hardening. However, materials produced by SLM may need different solution and/or aging treatments to optimize its microstructure and, correspondingly, their mechanical properties. For instance, some researchers [10] found that the AlSi10Mg alloy after only aging at 175 °C for 6 h shows better mechanical properties than high pressure die-cast (HPDC) parts after T6 treatment. Other work [11] has concluded that T6 heat treatments lead to a softening of this material produced by SLM instead of being hardened.

This article is part of the collection Welding, Additive Manufacturing and Associated NDT

✉ A. Iturrioz
aiturrioz@lortek.es

E. Gil
egil@lortek.es

M. M. Petite
mmpetite@lortek.es

F. Garciandia
fgarciandia@lortek.es

A. M. Mancisidor
ammancisidor@lortek.es

M. San Sebastian
msansebastian@lortek.es

[1] IK4-LORTEK, Arranomendia Kalea 4A, Ordizia, Spain

Furthermore, it is observed [4] that Si-rich particles precipitate during heat treatment and that the size of these particles has a strong influence on mechanical properties.

The aim of this work is to study the influence of various heat treatments (stress-relieving (300 °C) and solution treatment (450/550 °C with and without artificial aging)) on the microstructure of AlSi10Mg processed by SLM and its effect on mechanical properties. Thus, the validity of T6 treatments will be evaluated and the best heat treatment conditions will be identified for this material.

2 Materials and methods

Two batches of AlSi10Mg powder, with a particle size distribution between 20 and 63 μm, from different suppliers are studied. These powders are referred to as P1 and P2 powders. The chemical composition of these powders is given in Table 1. Their morphology and microstructure were observed by FE-SEM Ultra Plus of Zeiss manufacturer scanning electron microscope. Flowability was measured by a Hall flowmeter funnel. X-ray diffraction (XRD) measurements were performed on a PHILIPS PW1825 diffractometer (Cu, K_α) at 40 kV and 40 mA. The diffraction angle of 2θ varied from 20° to 110° with a step size of 0.05°. Tensile samples were manufactured with P2 powder in "z" building direction employing the optimum processing parameters determined previously for each powder with the aim to obtain parts with minimum porosity, free of defects and superior surface quality (Fig. 1). Relative density was determined by optical microscopy (GX51 Olympus) and using Image-J image analysis software. The parts were built in a SLM systems developed by SLM Solutions (model SLM 280HL). This machine is equipped with 400 W fiber laser and works with a protective atmosphere, being 0.2% the maximum oxygen allowable during manufacturing. The manufactured samples were subjected to several thermal treatments. A stress relieving heat treatment was performed with a heating rate of 10 °C/min until 300 °C for 2 h. Furthermore, specimens were solution treated at 450C and 550 °C during 2 h, followed by water quenching. Additionally, these samples were subjected to an artificial aging heat treatment at 180 °C for 12 h followed by water quenching. Tensile tests and hardness measurements of all samples were carried out in Zwick Roell Z100 tensile machine and Emco Test DuraScan durometer. As-built and heat-treated samples were cross-sectioned, polished, and etched with Keller's reagent. Afterwards, these samples were characterized by FE-SEM Ultra Plus scanning electron microscope of Zeiss manufacturer.

Table 1 Chemical composition of P1 and P2 powders (wt%)

	Al	Si	Mg	Fe	Cu	Mn	Cr
P1	Bal.	10.1	0.31	0.18	< 0.03	< 0.03	< 0.03
P2	Bal.	9.94	0.38	0.16	< 0.03	< 0.03	< 0.03
	Ni	Zn	Pb	Sn	Ti	O	
P1	< 0.03	< 0.03	< 0.03	< 0.03	< 0.02	0.08	
P2	< 0.03	< 0.03	< 0.03	< 0.03	< 0.02	0.04	

3 Results and discussion

3.1 Powder characterization

Two powders have been characterized in terms of microstructure, morphology, and humidity. Micrographs in Fig. 2 show that the morphology of P2 powder is more adequate for selective laser melting (SLM) process due to the fact that it is more spherical and has fewer satellites than P1. In addition, the humidity content of the P2 powder is significantly lower than that of P1 (Table 2). These features give better flowability to P2 (Table 2), which is a critical property to obtain a uniform layer deposition during processing by SLM [8]. Moreover, the packing density will optimize and, consequently, promote a higher contact area between particles and improve the consolidation process leading to a higher final density of the as-built sample. P2 also has lower internal porosity than P1 (Fig. 3). It is clear that the internal porosity of powders, which is caused by gas trapped during gas atomization, will contribute to increasing the porosity in the as-built samples [7], further deteriorating their mechanical properties [6]. In addition, the oxygen content of P2 powder is half of the P1 amount (Table 1). Thus, due to above-mentioned characteristics, as-built samples processed using P2 achieve higher final relative density (99.9%) than those processed with P1 (99.7%) (Table 2).

It is concluded that the physical characteristics of P2 powders are more suitable for processing final samples by SLM and, therefore, the as-built samples reported here are manufactured with this powder.

3.2 As-built sample characterization

It is well known that it is possible to evaporate the light elements during SLM due to the high energy density applied by the laser. Some authors [7] observed an evaporation of the half of Mg content during processing. The level of Mg is crucial because it is a key element to form Mg_2Si precipitates during heat treatments. Thus, as-built sample composition was measured in this alloy in order to evaluate if Mg evaporation occurred. Table 3 shows only the chemical composition of the elements which differ in composition from the powder (P2). Only Si and Mg contents are different from the powder. Si content is under the measurement uncertainty. A small loss of Mg element (0.04%) is measured. However, the amount of

Fig. 1 Tensile samples on the platform (**a**) and after removing from the platform (**b**)

this element is still within the target composition range for this alloy (0.2–0.45%).

Figure 4 shows the as-built microstructure of the tensile specimens. The microstructure reveals a cellular-dendritic solidification structure with α-Al matrix decorated with a network of Si-rich eutectic (Fig. 4). In this microstructure, three different zones can be distinguished by its cellular size in the XY plane (Fig. 4a). Each zone has been exposed to different temperature gradients, across the melt track, which induce this change in its cellular size. In the XZ plane (Fig. 4c, d), elongated grains indicate the thermal gradient direction. The coarse cellular zone corresponds to the melt pool boundary where the cooling rate is slower than at the melt pool center due to the Gaussian distribution of laser energy [4]. In the melt pool center, a fine cellular microstructure appears with cell sizes of 0.5–0.7 μm (Fig. 4b). These sizes are in good agreement with reported measurements for this material [4, 12]. A transition zone appears, a so-called heat-affected zone (HAZ) (Fig. 4a), which is associated with an overlap of melt pools and refusion of previously deposited layers [7, 12]. The same behavior was observed by several authors in other AlSi10Mg samples produced by SLM [4, 12, 13].

3.3 Microstructure evolution through heat treatments

The microstructure becomes coarser after heat treatment. Si distribution changes and this element, instead of being around α-Al grain boundaries in the supersaturated matrix as in the as-built samples (Fig. 4), forms polygonal precipitates. Similar microstructures have been observed by other researchers [4, 14]. The size of these phases increases as the heat treatment temperature rises (Fig. 5). After stress relieving at 300 °C for 2 h, Si particles have a size between 0.1 and 0.6 μm. However, particle size increases significantly, when a solution heat treatment is performed above 450 °C. After heat treatment at 450 and 550 °C, particle size is in the range of 0.4–2 μm and 2–6 μm, respectively. Other authors [4] reported an average particle size of about 3 and 4.5 μm at 450 and 550 °C, respectively. Furthermore, while the heat treatment temperature increases, the number of Si particles decreases, probably owing to Ostwald ripening phenomenon. On the other hand, the artificial aging does not result in significant Si particle coarsening (Fig. 5i, h). A chemical analysis of these particles is shown in Fig. 5g.

It is worth noting that after heat treatment at 550 °C, an additional phase is identified. This phase differs from the Si

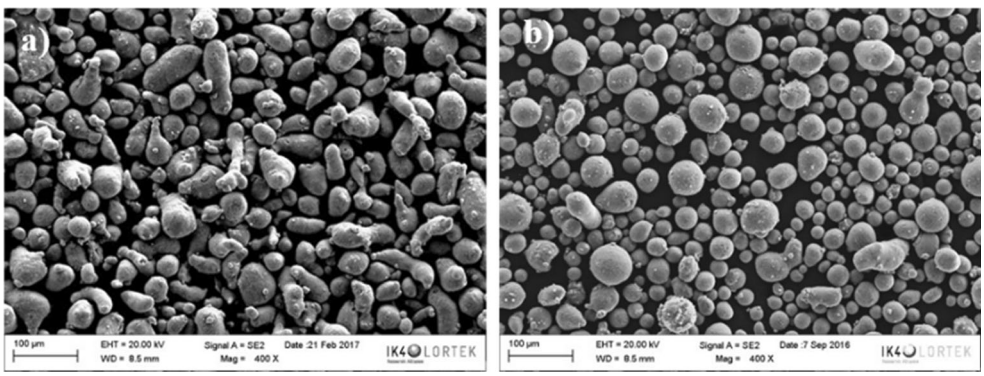

Fig. 2 Comparison of powder morphology between **a** P1 and **b** P2

Table 2 Humidity and flowability of powders P1 and P2 and the maximum density values of as-built samples processed with them

	P1	P2
Humidity (%)	< 10	4.5
Flowability	100 s/50 g	80 s/50 g
Max. density (%)	99.76	99.9

particles in its morphology, which is a rod-like shape. This phase showed less adherence with the matrix than Si particles (Fig. 5e, red arrows). It was not possible to identify these phases by EDS or X-Ray analysis because all of them were pulled from the matrix during sample preparation (Fig. 6). Sample preparation should be improved to unambiguously identify this phase. Other researchers [13] observed precipitates with similar size and shape after a solution heat treatment at 520 °C and artificial aging at 160 °C in AlSi10Mg produced by SLM. They referred to these precipitates as Mg_2Si precipitates. It is observed that another Al-Si-Mg-based alloy (Al-1.29Si-1.13 Mg), after casting and subsequent heat treatments of homogenization (530 °C, 24 h), annealing (450 °C, 24 h) with final water quenching, showed this same type of particle with maximum size around 5 μm. In this study [14], these precipitates were identified as rod-like β Mg_2Si precipitates. Thus, it seems that rod-like precipitates which appeared after solution treatment at 550 °C are most likely to be Mg_2Si precipitates. Nevertheless, the presence of other intermetallic Al-Fe-Si(-Mg) phases with similar shape cannot be excluded since they are observed in other conventional Al alloys. In fact, other work [15] has confirmed the presence of β-Al_5FeSi in Al-Si-Mg cast alloy and it is noted [16] that these intermetallic precipitates have a low adhesion with the matrix. It is shown that these rod-like particles remain after the artificial aging almost without size variation (Fig. 5i, red arrows).

X-ray analysis was performed in order to evaluate the evolution of the phases formed during heat treatments and identify them (Fig. 6). Si and Al crystallographic phases are only indexed (reference codes of 01-071-3899 and 01-071-4624, respectively). Thus, no Mg_2Si peaks were detected probably because there was no sufficient quantity to allow identification. Other work [17] has also failed to identify these precipitates by XRD analysis although they have hypothesized that they are present even in as-built condition. On the other hand, Si peaks of the heat-treated samples have higher intensities than those of the as-built parts due to the fact that there is a decrease of Si in solid solution in the Al matrix after heat treatments due to the formation of Si precipitates. This is consistent with the observed microstructure (Fig. 5). In addition, Si peaks are more intense as the temperature increases since there is a higher volume fraction of these precipitates (Fig. 5).

Table 3 Chemical composition of as-built sample

Al	Si	Mg
Bal.	9.19	0.34
Percentage relative to powder (%)	92.5	89.5

3.4 Evolution of mechanical properties after heat treatments

Tensile curves are shown in Fig. 7a and the values of ultimate tensile strength (UTS) and ductility from these curves are shown in Fig. 7b. Figure 7 provides a summary of the mechanical response as a function of temperature. The highest tensile and yield strength are achieved in the as-built sample due to its fine cellular microstructure obtained due to a rapid solidification process during SLM. This behavior is consistent with other studies of AlSi10Mg alloy produced by SLM [4, 11]. The as-built UTS value (382 MPa) achieved in this work is in the range of those obtained in the literature (333–434 MPa) [4, 11, 17]. It is confirmed by other research that Mg_2Si is also present in as-built samples [4, 18]. Thus, this high dispersion in tensile strength values could be attributed to differences in composition such as Mg content which is the limiting reactant to form Mg_2Si precipitates [4]. However, the ductility of the as-built sample is very low (2%).

A stress-relieving heat treatment was carried out to improve the ductility. After this treatment, the ductility increases

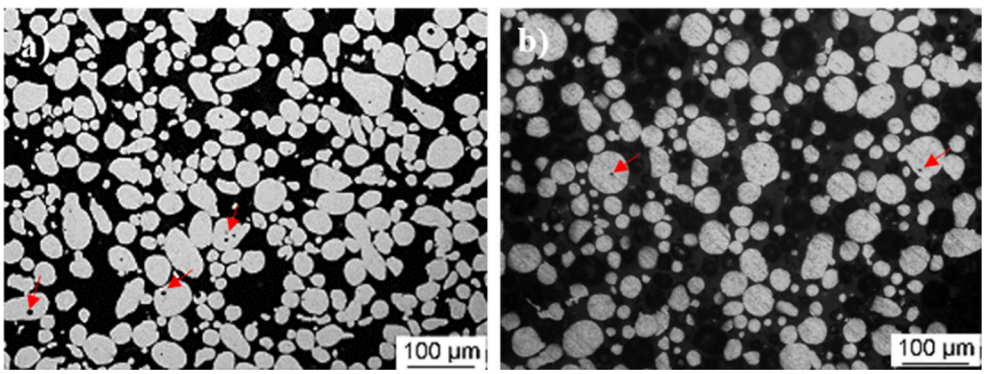

Fig. 3 Polished powder showing the internal porosity of P1 (**a**) and P2 (**b**) powders

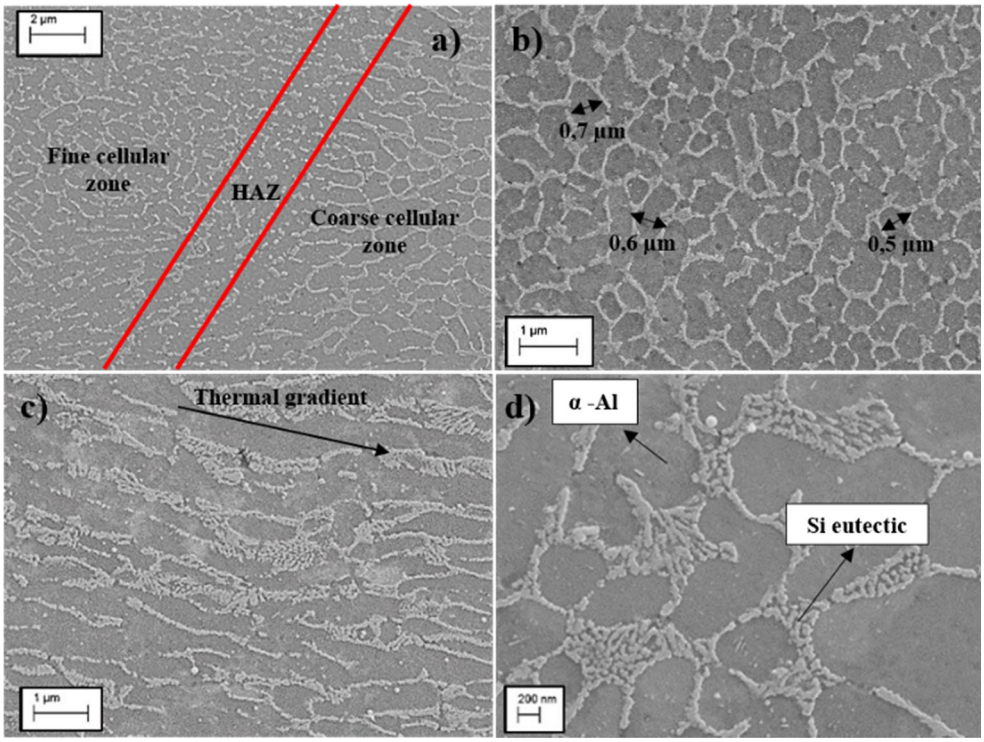

Fig. 4 As-built sample microstructure showing fine cellular-dendritic solidification structure, **a** microstructure showing three zones (XY section, top view), micrographs showing **b** the fine cellular zone (XY) and **c** columnar grains indicating the thermal gradient direction (XZ), **d** micrograph at high magnification identifying different chemical phases (XZ)

dramatically up to 17% and tensile strength drops significantly from 382 to 220 MPa. This is in line with the changes detected in microstructure where a high density of small Si-rich precipitates form. When the temperature of the solution treatment rises, the ductility decreases probably due to the formation and growth of polygonal Si-rich particles. However, further work on fracture analysis is required to verify this point. Even if the UTS and yield strength decrease after 450 °C, specimens heat treated at 550 °C exhibited a substantial increase in UTS, from 189 MPa (at 450 °C) to 248 MPa. Nevertheless, W. Li et al. [4] observed a decrease in tensile strength from 282 to 168 MPa after 450 and 550 °C, respectively. They related this drop in UTS values to the lack of Si in the matrix, which reduces solid solution strengthening, and to the shorter distance between Si particles.

In the present work, a significant improvement in UTS values is observed after increasing the solution temperature to 550 °C. This behavior could be explained by the presence of the rod-like phase in the microstructure of specimens investigated in this work. On the another note, artificial aging of both samples subjected to solution treatments results in significant increase in tensile and yield strength while the ductility values are reduced to 11 and 9% in samples treated at 450 and 550 °C, respectively (Fig. 7b, c). The effect of aging in improvement of mechanical properties is probably due to higher Mg_2Si nanoprecipitate formation, although they cannot be identified by X-ray diffraction. TEM characterization should be carried out to identify and quantify their density. This precipitation during the aging process is well known [19]. W. Li et al. [4] measured tensile strength of 197 and 187 MPa in AlSi10Mg alloy after the same T6 treatment at 450 and 550 °C, respectively. The reason for these low values in comparison with those reported here is due to the lack of Mg_2Si precipitation after aging, according to XRD analysis. Moreover, other authors [11] after a T6 treatment (520 °C, 1 h and artificial aging at 160 °C during 6 h), obtained a tensile strength of 292 MPa which is in accordance with the value obtained in this work after 550 °C solution treatment and artificial aging.

The as-built sample, which has the finest microstructure, shows the highest microhardness (127 ± 5 $HV_{0.5}$) due to the Hall-Petch effect (Fig. 7d). This value is in good agreement with other measurements carried out by other researchers (127 ± 3 $HV_{0.5}$) [12] and it is slightly lower than the one achieved in the other study (133 ± 5 HV1) [4]. Nevertheless, this hardness is higher than the typical hardness values obtained in as-cast condition samples processed by high pressure die-casted (HPDC) and significantly higher than conventional AlSi10Mg cast alloys' hardness values (Table 4). Material was substantially softened after heat treatments due to the coarsening of microstructure. The lower value appeared after solution heat treatment at 550 °C. Nonetheless, an artificial aging of this specimen causes a dramatic rise in hardness value from 70 to 101 $HV_{0.5}$, probably due to the formation of Mg_2Si nanoprecipitates, which induces Orowan strengthening.

Although the highest UTS (382 ± 10 MPa) and hardness values (127 ± 5 $HV_{0.5}$) were obtained in as-built sample, the ductility is very low (2.3 ± 0.2%). Thus, a better combination

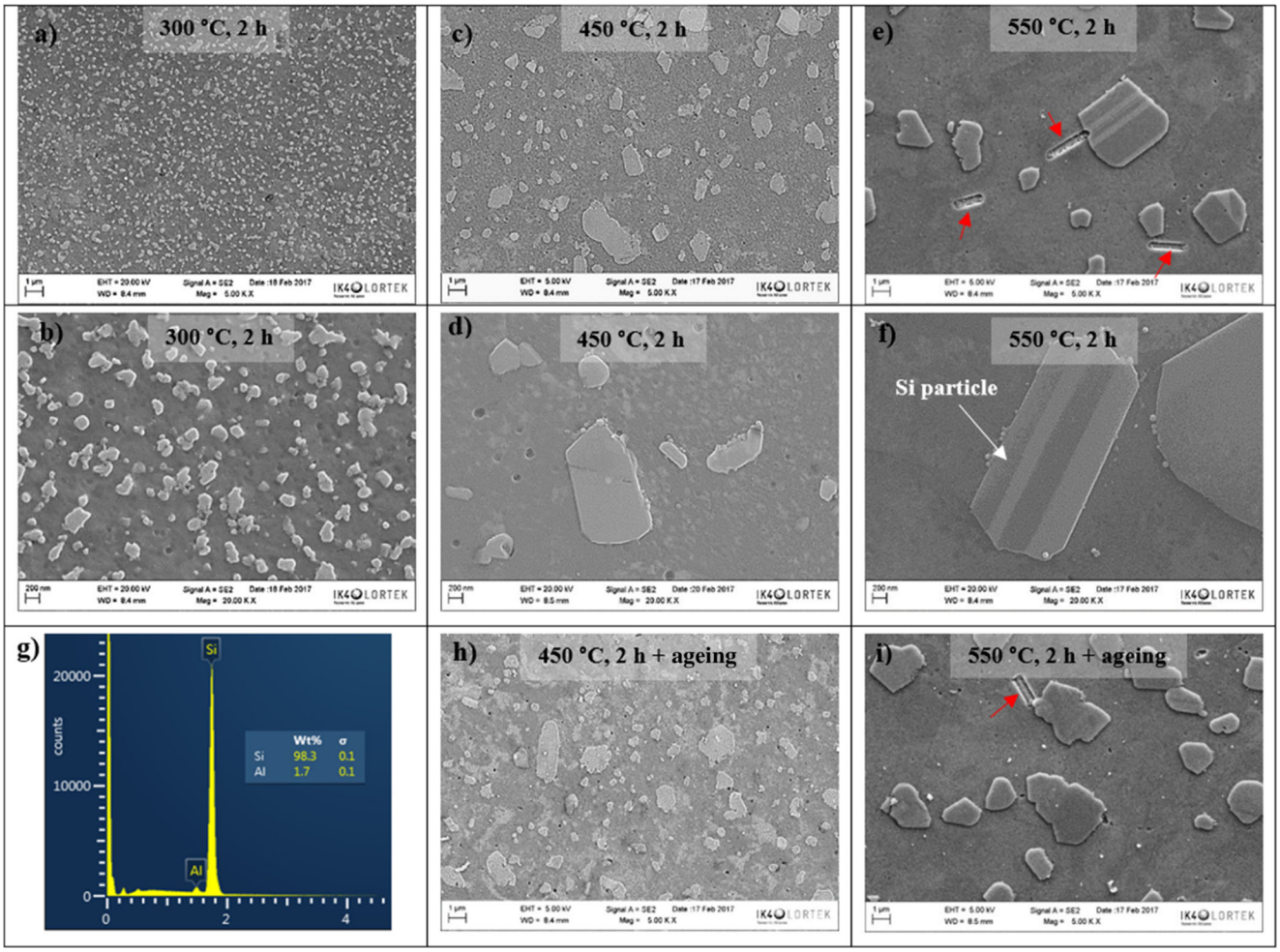

Fig. 5 Microstructures after **a**, **b** stress-relieving heat treatment (300 °C, 2 h), **c**, **d** solution heat treatments at 450 °C, 2 h, and **e**, **f** 550 °C, 2 h; and aging heat treatments of (h) 450 °C, 2 h + 180 °C, 12 h and **i** 550 °C, 2 h + 180 °C, 12 h. Chemical analysis (EDS spectrum) of typical Si particles is shown (g)

of mechanical properties was achieved after the T6 treatment, consisting of a solution heat treatment at 550 °C and artificial aging. This sample exhibited a tensile strength, yield strength, hardness, and ductility of 307 ± 8 MPa, 248 ± 2 MPa, 101 ± 4 HV0.5, and 9 ± 3%, respectively. This property combination is better than that achieved in as-cast AlSi10Mg alloy and die cast A360 alloy (Table 5). Thus, the SLM material in this study, after optimum T6 heat treatment, achieved significantly better hardness and ductility relative to conventional Al-Si-Mg as-cast alloys at a comparable tensile strength.

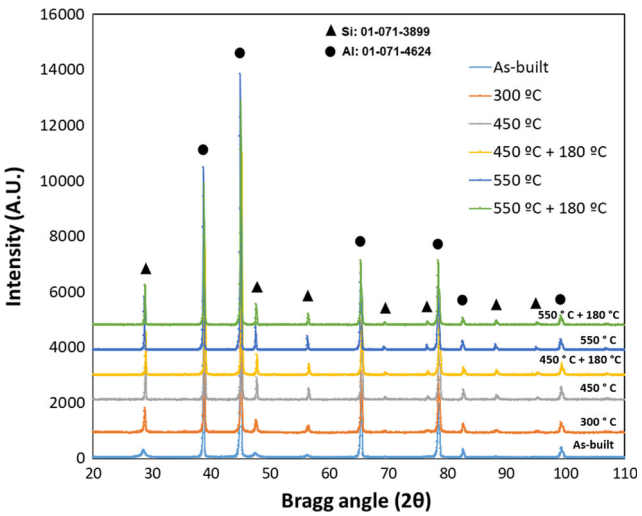

Fig. 6 X-ray analysis of AlSi10Mg as-built sample and after all heat treatments

4 Conclusions

The P2 powder evaluated in this study was selected as the best powder to be used in SLM process due to the fact that it has better quality regarding morphology, porosity, humidity, and oxygen content. The as-built samples produced with this powder achieved a relative density of 99.9%. In these samples, Mg content remains almost unaffected which means that there is

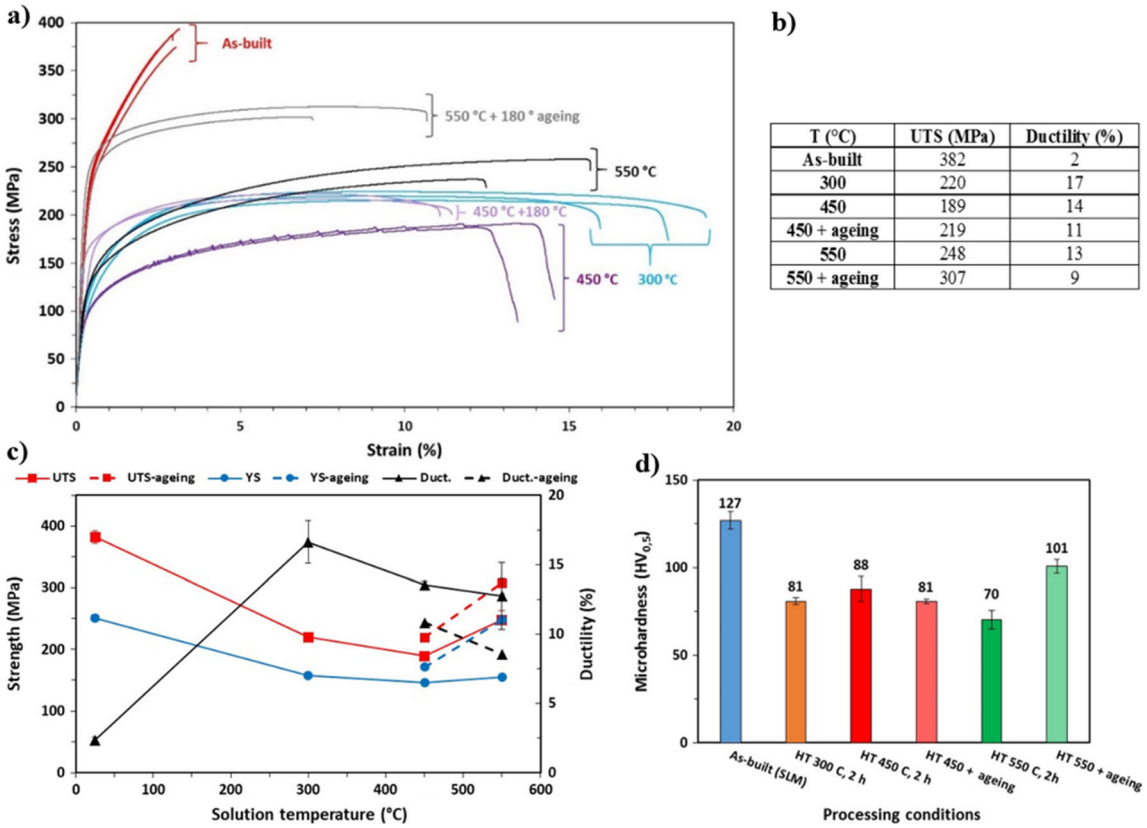

T (°C)	UTS (MPa)	Ductility (%)
As-built	382	2
300	220	17
450	189	14
450 + ageing	219	11
550	248	13
550 + ageing	307	9

Fig. 7 **a** Tensile curves of all samples. **b** Table showing ultimate tensile strength (UTS) and ductility average values of all samples. **c** Ultimate tensile strength (UTS), yield strength (YS), and ductility values through heat treatments (note that values at 25 °C correspond to as-built sample and that dashed lines are related to samples after artificial aging). **d** Hardness values of all samples

not a significant evaporation of this element during SLM processing.

The SLM microstructure of AlSi10Mg alloy is very fine with α-Al grains boundaries decorated with Si-rich eutectic. This allows the as-built sample to achieve the best tensile strength and hardness values. After heat treatments, Si forms polygonal precipitates whose size increases as the temperature increases. This results in a decrease in tensile strength and hardness up to 450 °C. However, after heat treatment at 550 °C, rod-like precipitates (probably Mg_2Si or Al-Fe-Si intermetallics) appear in the microstructure apart from the Si-rich particles. This provides a significant improvement in tensile strength in comparison with specimens heat treated at 450 °C.

The maximum ductility (17%) is achieved in the sample after a stress-relieving treatment (300 °C), where Si-rich particles have a size between 0.1–0.6 μm, but tensile strength values are not optimal at this stage. Aging effects on mechanical properties are considerable even if there is not a significant change in observed microstructure. Tensile and yield strength after heat treatment increase substantially, probably due to additional precipitation of Mg_2Si nanoparticles. The best improvement occurred after aging the previously heat treated sample (550 °C, 2 h) at 180 °C which led to a tensile strength of 307 ± 8 MPa and hardness of 101 ± 4 $HV_{0.5}$, with ductility of 9 ± 3%. This heat treatment produces a better combination of hardness and ductility than AlSi10Mg as-cast alloys of equivalent tensile strength.

It is concluded that T6 treatments of AlSi10Mg processed by SLM provides an optimum combination of tensile strength and ductility. Based on the results of this study, the best T6

Table 4 Hardness values obtained in AlSi10Mg alloy by different processing types

Processing type	Hardness (HV)	Ref.
SLM	127	This work
HPDC	95–105	[10]
Conventional cast alloy	86	[17]

Table 5 Mechanical data of A360 alloy and AlSi10Mg alloy processed by alternative and conventional procedures

Processing type	UTS (MPa)	Ductility (%)	Ref.
AlSi10Mg SLM + T6	307 ± 8	9 ± 3	This work
AlSi10Mg cast-alloys	300–317	2.5–3.5	[17]
AlSi10Mg cast-alloy + T6	263	–	[20]
Die cast A360	320	3	[11, 21]

treatment was identified as solution treatment at 550 °C for 2 h followed by aging at 180 °C for 12 h.

References

1. Li Y, Gu D (2014) Parametric analysis of thermal behavior during selective laser melting additive manufacturing of aluminum alloy powder. Mater Des 63:856–867
2. Voncina M, Mrvar P, Medved J (2005) Thermodynamic analysis of AlSi10Mg alloy = termodinamicna analiza zlitine AlSi10Mg. RMZ-Mater Geoenviron 52(3):621–633
3. Jordović B, Nedeljković B, Mitrović N, Živanić J, Maričić A (2014) Effect of heat treatment on structural changes in metastable AlSi10Mg alloy. J Min Metall Sect B Metall 50(2):133–137
4. Li W, Li S, Liu J, Zhang A, Zhou Y, Wei Q, Yan C, Shi Y (2016) Effect of heat treatment on AlSi10Mg alloy fabricated by selective laser melting: microstructure evolution, mechanical properties and fracture mechanism. Mater Sci Eng A 663:116–125
5. Louvis E, Fox P, Sutcliffe CJ (2011) Selective laser melting of aluminium components. J Mater Process Technol 211(2):275–284
6. Kempen K (2015) "Expanding the materials palette for Selective Laser Melting of metals," Thesis, KU Leuven University
7. Aboulkhair NT, Everitt NM, Ashcroft I, Tuck C (2014) Reducing porosity in AlSi10Mg parts processed by selective laser melting. Addit Manuf 1:77–86
8. Aboulkhair NT, Maskery I, Ashcroft I, Tuck C, Everitt NM (2015) "The role of powder properties on the processability of Aluminium alloys in selective laser melting," Laser Manuf. Conf. 2015, no. JUNE
9. Lumley RN, Polmear IJ, Groot H, Ferrier J (2008) Thermal characteristics of heat-treated aluminum high-pressure die-castings. Scr Mater 58(11):1006–1009
10. Kempen K, Thijs L, Van Humbeeck J, Kruth J-P (2015) Processing AlSi10Mg by selective laser melting: parameter optimisation and material characterisation. Mater Sci Technol 31(8):917–923
11. Aboulkhair NT, Maskery I, Tuck C, Ashcroft I, Everitt NM (2016) The microstructure and mechanical properties of selectively laser melted AlSi10Mg: the effect of a conventional T6-like heat treatment. Mater Sci Eng A 667:139–146
12. Thijs L, Kempen K, Kruth JP, Van Humbeeck J (2013) Fine-structured aluminium products with controllable texture by selective laser melting of pre-alloyed AlSi10Mg powder. Acta Mater 61(5):1809–1819
13. Aboulkhair NT, Tuck C, Ashcroft I, Maskery I, Everitt NM (2015) On the precipitation hardening of selective laser melted AlSi10Mg. Metall Mater Trans A 46(8):3337–3341
14. Phongphisutthinan C, Tezuka H, Kobayashi E, Sato T (2013) Effects of β-Mg2Si precipitates on semi-solid microstructures of wrought Al–Mg–Si based alloys produced by deformation-semi-solid-forming process. Mater Trans 54(4):609–617
15. Dybowski B, Szymszal J, Poloczek Ł, Kiełbus A (Jan. 2016) Influence of the chemical composition on electrical conductivity and mechanical properties of the hypoeutectic Al-Si-Mg alloys. Arch Metall Mater 61(1):353–360
16. Dobkowska A, Adamczyk-Cieślak B, Mizera J, Kurzydłowski KJ, Kiełbus A (2016) The comparison of the microstructure and corrosion resistance of sand cast aluminum alloys. Arch Metall Mater 61(1):209–212
17. Kempen K, Thijs L, Van Humbeeck J, Kruth J-P (2012) Mechanical properties of AlSi10Mg produced by selective laser melting. Phys Procedia 39:439–446
18. Lam LP, Zhang DQ, Liu ZH, Chua CK (2015) Phase analysis and microstructure characterisation of AlSi10Mg parts produced by selective laser melting. Virtual Phys Prototyp 10(4):207–215
19. Abis S, Caciuffo R, Coppola R, Magnani M, Rustichelli F, Stefanon M (1986) Small angle neutron scattering investigation of the ageing process in Al-Mg-Si alloy. Phys B+C 136(1–3):469–472
20. Tradowsky U, White J, Ward RM, Read N, Reimers W, Attallah MM (2016) Selective laser melting of AlSi10Mg: influence of post-processing on the microstructural and tensile properties development. Mater Des 105:212–222
21. Read N, Wang W, Essa K, Attallah MM (2015) Selective laser melting of AlSi10Mg alloy: process optimisation and mechanical properties development. Mater Des 65:417–424